The mechanics of unrest at Long Valley caldera, California : 1. Modeling the geometry of the source using GPS, leveling and two-color EDM data

M. Battaglia [a,*], P. Segall [a], J. Murray [a], P. Cervelli [a], J. Langbein [b]

[a] *Department of Geophysics, Stanford University, Stanford, CA 94305-2215, USA*
[b] *U.S. Geological Survey, 345 Middlefield Rd, Menlo Park, CA 94025, USA*

Abstract

We surveyed 44 existing leveling monuments in Long Valley caldera in July 1999, using dual frequency global positioning system (GPS) receivers. We have been able to tie GPS and leveling to a common reference frame in the Long Valley area and computed the vertical deformation by differencing GPS-based and leveled orthometric heights. The resurgent dome uplifted 74 ± 7 cm from 1975 to 1999. To define the inflation source, we invert two-color EDM and uplift data from the 1985–1999 unrest period using spherical or ellipsoidal sources. We find that the ellipsoidal source satisfies both the vertical and horizontal deformation data, whereas the spherical point source cannot. According to our analysis of the 1985–1999 data, the main source of deformation is a prolate ellipsoid located beneath the resurgent dome at a depth of 5.9 km (95% bounds of 4.9–7.5 km). This body is vertically elongated, has an aspect ratio of 0.475 (95% bounds are 0.25–0.65) and a volume change of 0.086 km^3 (95% bounds are 0.06–0.13 km^3). Failure to account for the ellipsoidal nature of the source biases the estimated source depth by 2.1 km (35%), and the source volume by 0.038 km^3 (44%).
© 2003 Elsevier B.V. All rights reserved.

1. Introduction

The Long Valley area (Fig. 1) has been active

---

* Corresponding author. Present address: UC Berkeley Seismological Laboratory, 215 McCone Hall, Berkeley, CA 94720-4760, USA. Fax: +1-510-643-5811.
   E-mail addresses: battag@seismo.berkeley.edu (M. Battaglia), segall@pangea.stanford.edu (P. Segall), jrmurray@pangea.stanford.edu (J. Murray), cervelli@pangea.stanford.edu (P. Cervelli), langbein@shasta.wr.usgs.gov (J. Langbein).

for the past 3 million years. Rhyolite lava eruptions from 2.1 to 0.8 Ma formed Glass Mountain on the northeast rim of the present caldera (Metz and Mahood, 1985). The Glass Mountain eruptions, which were fed by a large, chemically evolving magma chamber in the shallow crust (Knesel and Davidson, 1997), culminated 0.76 Ma ago in a cataclysmic caldera forming eruption (van den Bogaard and Schirnick, 1995). This massive eruption resulted in the deposition of 600 km^3 of Bishop Tuff and the simultaneous subsidence of the magma chamber roof creating the present 17 by
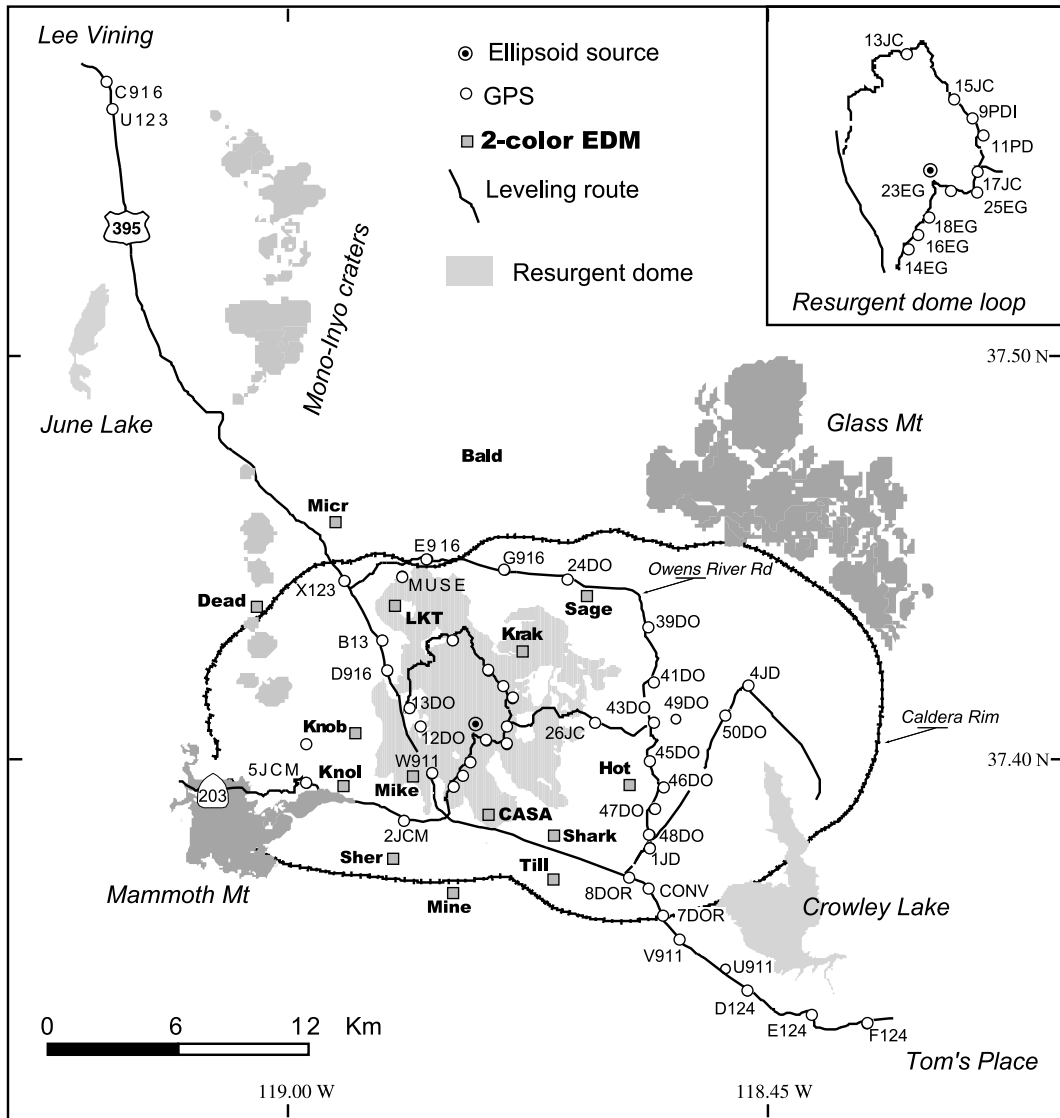
Fig. 1. Map of Long Valley caldera geodetic networks.

32 km, oval depression of Long Valley caldera. Between 0.76 and 0.6 Ma ago, uplift of the caldera floor and eruption of flows of rhyolite lava formed the resurgent dome (Bailey, 1989). The most recent eruptive activity occurred 600 yr ago along the Mono–Inyo craters volcanic chain (Sieh and Bursik, 1986). In May of 1980, a strong earthquake swarm struck the southern margin of Long Valley caldera, marking the onset of the current period of unrest (Bailey and Hill, 1990).

This ongoing unrest includes recurrent earthquake swarms and uplift of the resurgent dome within the central section of the caldera (Fig. 2). According to the latest leveling survey, in September 1997 the resurgent dome stood roughly 0.72 m higher than in 1975 (Fig. 2). After a sharp increase in the deformation rate during the summer–fall of 1997, the caldera reverted to a state of low activity with no significant deformation since the spring of 1998 (Figs. 3 and 4).
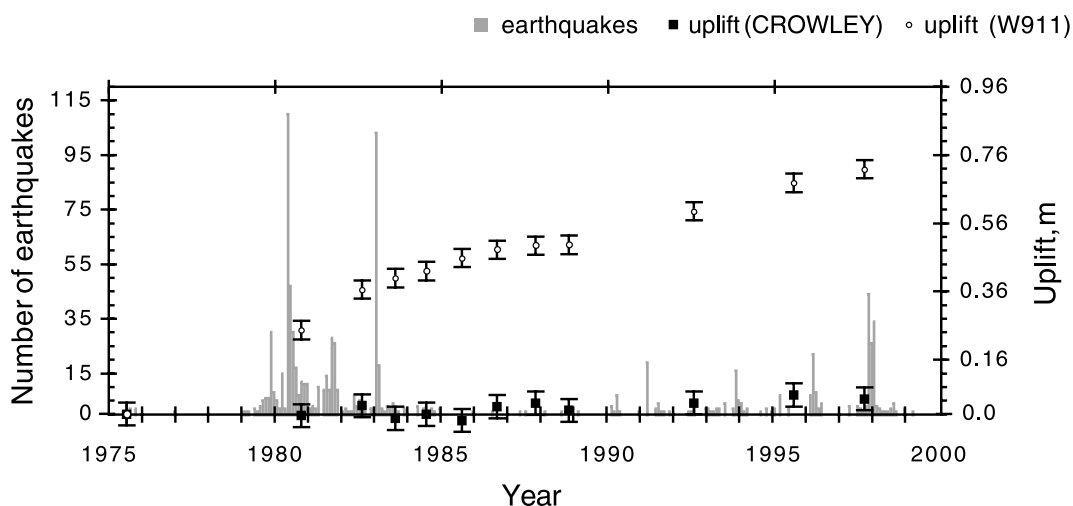
Fig. 2. Long Valley caldera unrest. The plot shows the number of M > 3.0 monthly earthquakes and the uplift at two bench marks; W911 bench mark near the apex of the resurgent dome and CROWLEY bench mark several km outside the caldera. Leveling data provided by the USGS Cascades Volcano Observatory (Dzurisin, personal communication). Earthquake data between 1979 and 2000 provided by the USGS Long Valley Observatory (Hill, personal communication) and the Northern California Earthquake Data Center (NCEDC), on line at http://quake.geo.berkeley.edu.

The U.S. Geological Survey (USGS) started an intensive geodetic monitoring program in Long Valley between 1980 and 1982 (Bailey and Hill, 1990). Data collected by the USGS include leveling surveys from 1980 to 1997 (Denlinger and Riley, 1984; Savage et al., 1987; Langbein et al., 1995; see Table 1), and measurements of horizontal deformation using a two-color geodimeter (from 1985; Langbein, 1989; Langbein et al., 1993; Langbein et al., 1995) and global positioning system (GPS) (from 1994; Marshall et al., 1997). The last complete leveling of Long Valley caldera occurred in July–August 1992. A network of continuously operating GPS receivers monitors crustal deformation in the caldera (Dixon et al., 1997).

To bring up to date the direct measurement of vertical deformation within the caldera, we surveyed 44 of the existing leveling monuments in Long Valley in July 1999 using dual frequency GPS receivers (Fig. 1). Centimeter precision in the vertical can be achieved with GPS using standard geodetic hardware and software (Zilkoski et al., 1997). A GPS survey does not require a trained crew and is less time-consuming and more cost-effective than a leveling survey.

Several sources of deformation have been identified in Long Valley caldera, even if their geometry, depth and volume are not yet well constrained. Surveys of two-color EDM and leveling networks indicate that the principal sources of deformation are the intrusion of a magma body beneath the resurgent dome, and right lateral strike slip within the south moat of the caldera (Denlinger and Riley, 1984; Savage et al., 1987; Savage, 1988; Langbein et al., 1995). In addition, there is evidence for dike intrusion beneath the south moat (Savage and Cockerham, 1984; Savage et al., 1987; Langbein et al., 1995) and Mammoth Mt (Hill et al., 1990; Sorey et al., 1993; Langbein et al., 1995). Radar interferometry (Thatcher and Massonet, 1997; Fialko et al., 2001), GPS surveys (Marshall et al., 1997) and gravity measurements (Battaglia et al., 1999) confirm the intrusion beneath the resurgent dome. According to Langbein et al. (1995), Thatcher and Massonet (1997) and Marshall et al. (1997), the primary source of inflation is located beneath the resurgent dome at 5.5–7 km depth. Langbein et al. (1995) identified a secondary source beneath the south moat at a depth between 10 and 20 km. Tiampo et al. (2000) located the primary source
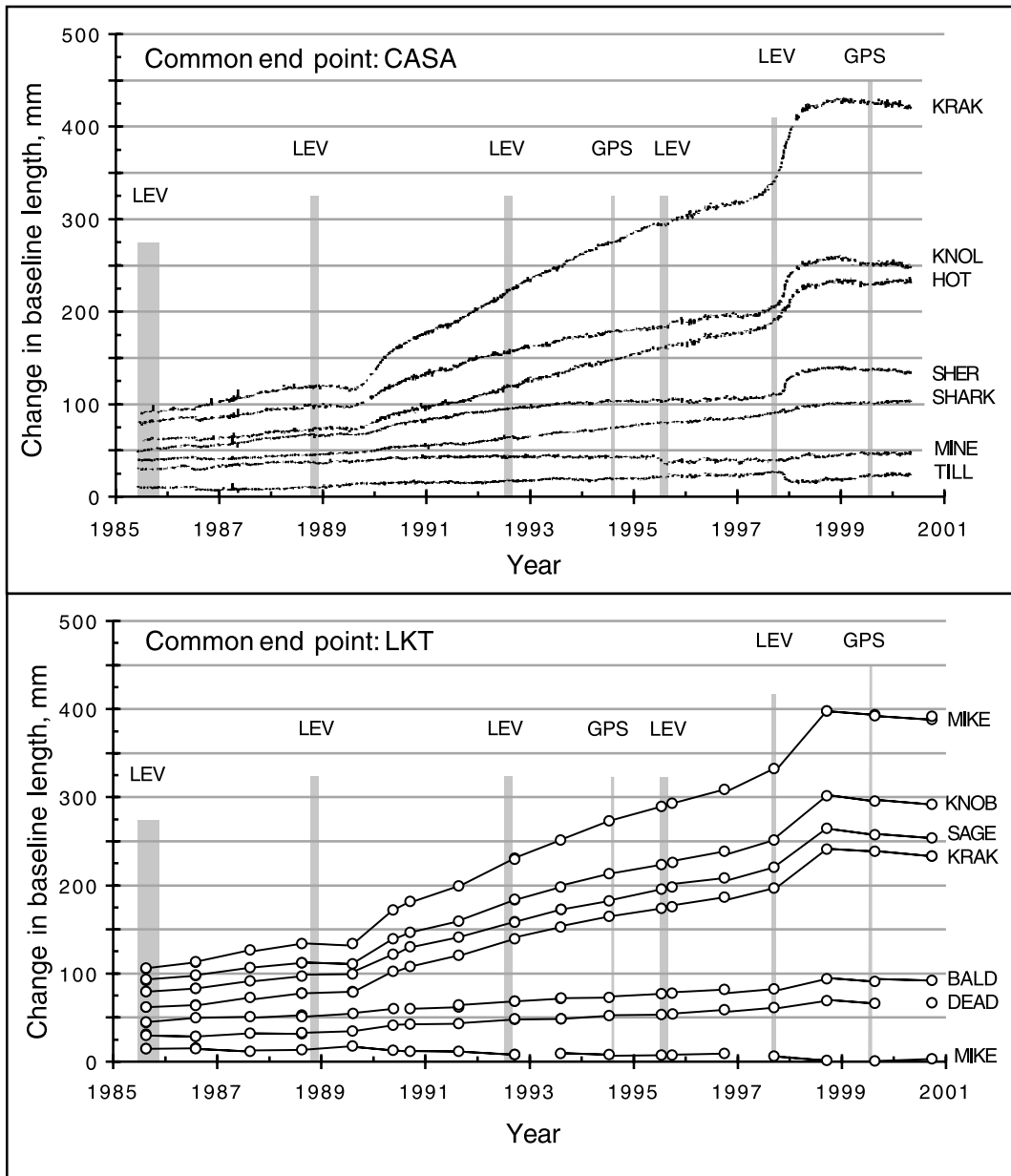
Fig. 3. Horizontal deformation at Long Valley from two-color EDM data. The data show the abrupt increase in deformation rate during the fall of 1997, and a slight reversal in trend after the spring of 1998. Superposed on the horizontal deformation data is the time span (gray bars) of the leveling (LEV) and GPS surveys mentioned in the text.

beneath the resurgent dome at 9.6–9.9 km depth, and the secondary source beneath the south moat at 7.3–11.8 km depth, with the volume of the primary source 5–10 times larger than the volume of the secondary source. Inversion of trilateration (Estrem et al., 1985) and gravity data (Battaglia et al., 1999) suggests a deeper (10–14 km) location for the intrusion beneath the resurgent dome.

This work has two goals. The first is to use GPS and leveling data to determine uplift within
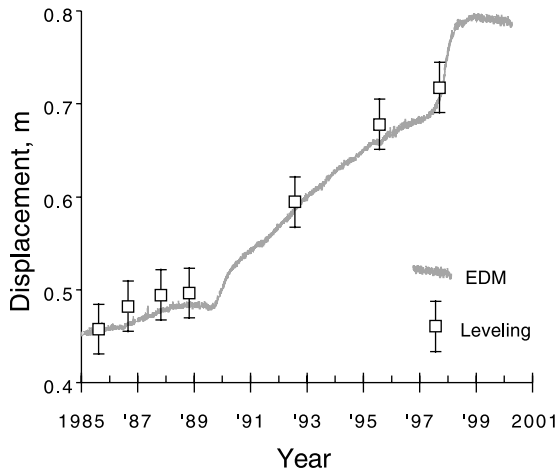
Fig. 4. The time series of the horizontal deformation along the CASA–KRAK baseline is very similar to the history of the vertical deformation at the resurgent dome (bench mark W911). The USGS has used this similarity to get a qualitative estimate of the vertical deformation at the resurgent dome when a direct measurement was missing.

the caldera. Deformation measurements can bound volume changes within the crust, not the cause of those volume changes. Gravity change measurements combined with deformation measurements can allow one to infer the density of the intruded material, thereby more tightly defining the cause of unrest (Berrino et al., 1992; Rymer, 1994). Before gravity change data can be used to estimate the density of the intrusion (Battaglia et al., same issue), they must be corrected for the effect of uplift (the free-air effect) (e.g. Jachens and Roberts, 1985). The vertical displacement field derived by differencing GPS and leveling can be used to correct gravity change measurements. The second goal is to bound the depth and geometry of the intrusion beneath the resurgent dome. Because sources with different geometry can have very similar vertical deformation profiles, but distinct horizontal deformation patterns (Dieterich and Decker, 1975), we invert both the vertical and horizontal displacements. To improve the signal-to-noise ratio, we model the inflation period from 1985 to 1999, the longest time interval for which both horizontal and vertical deformation data are available. We also evaluate the application of both spherical and ellipsoidal models.

2. Comparing GPS and leveling

Before we can compare our GPS measurements with leveled heights to obtain vertical displacements, we must transform the heights into the same reference frame (Fig. 5). The reference surface for leveling is the geoid, an equipotential surface closely identified with mean sea level (Rapp, 1980). To obtain a homogeneous set of elevations from different leveling surveys, raw leveling heights must be referenced to a common vertical datum. The present vertical datum for the United States is the North American Vertical Datum of 1988 (NAVD88). NAVD88 elevations are expressed by Helmert orthometric heights, which can be computed using the Helmert orthometric reduction (Zilkoski et al., 1992). GPS solutions, on the other hand, produce a set of XYZ coordinates that do not directly express the notion of height. To obtain heights from GPS solutions, the XYZ coordinates must be transformed into geodetic latitude, longitude and ellipsoidal heights. This transformation is usually performed using the World Geodetic System WGS84 ellipsoid model (Snay and Soler, 2000). In the continental United States, horizontal coordinates in WGS84 are practically identical to those of the present North American horizontal Datum of 1983 (NAD83); the two systems agree at the 0.1-mm level (Langley, 1992). Geoid and ellipsoid surfaces, however, do not coincide. The vertical distance between the ellipsoid and the geoid is called the geoid height. GPS heights can be transformed into the same reference frame as leveled heights
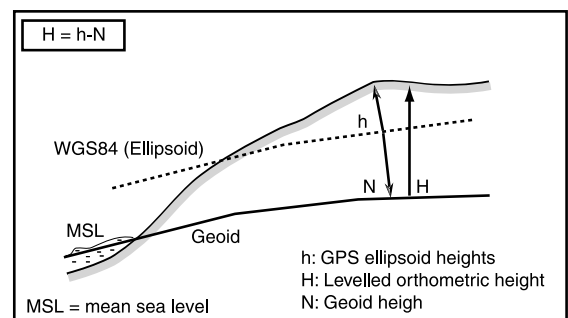

Fig. 5. Relationship between the ellipsoid heights h, orthometric heights H, and geoid height N.

by using an appropriate geoid height model (Smith and Milbert, 1999). Geoid height models developed by the National Geodetic Survey (NGS) enable one to directly convert between NAD83 GPS heights and NAVD88 leveling heights (Milbert and Smith, 1996).

3. Leveling and two-color EDM data

Leveling, in which height differences between stations are measured with a precise optical level, has been used to measure the vertical deformation along the 65-km-long line along Highway (Hwy) 365 from Tom's Place to Lee Vining and along several other routes within the caldera (Fig. 1; Table 1). The bench mark C916 (Fig. 1) is the elevation datum for all the leveling surveys. The Hwy 395 route was surveyed in 1932, 1957, 1975, 1980, each summer from 1982 to 1988, and again in 1992, 1995 and 1997 (Denlinger and Riley, 1984; Savage et al., 1987; Langbein et al., 1995). Complete leveling of the caldera occurred each summer from 1982 to 1986, and in 1988 and 1992 (Langbein et al., 1995). The leveling surveys have been run to standards equal to those required for second-order, class II levels or for first-order, class II levels. The standard error for each elevation difference can be taken to be 3 mm/$L^{1/2}$, where L is the distance between bench marks in km (Langbein et al., 1995). Leveling observations were corrected for rod scale and temperature, level collimation, and for astronomic, refraction and magnetic effects (Balazs and Young, 1982). Leveling surveys were not referenced to the NAVD88 datum because the USGS was only interested in monitoring relative elevation changes within the caldera.

Horizontal deformation is monitored by measuring changes in the baseline lengths of the two-color geodimeter network (Fig. 1). Baseline lengths are measured from several times weekly to several times yearly (Fig. 3). The more frequently measured lines, including the stations KNOL, SHER, MINE, TILL, SHARK, HOT and KRAK, are observed from the central monument CASA (see Fig. 1). The other stations (MIKE, KNOB, DEAD, MICR, BALD, SAGE

and KRAK) are observed from the LKT monument (see Fig. 1), and are measured less frequently. In total there are 14 baselines with measurements that span the 1985–1999 inflation period (Table 2). The USGS has used the change in the length of the CASA–KRAK baseline to estimate the vertical deformation at the resurgent dome when direct measurements are unavailable. This application is based on the similarity between the history of vertical deformation recorded by the leveling surveys and the horizontal deformation along the CASA–KRAK EDM baseline (see Fig. 4). Methods used to extract the displacement and its error for each of the baselines are described in Langbein et al. (1993) and Langbein et al. (1995). The formal instrument variance of the two-color measurements is $\sigma^2 = a^2 + b^2 L^2$, where $a = 0.3$ mm and $b = 0.12$ ppm of the baseline length L (Langbein et al., 1993). This does not account for any time-dependent noise due to local motion of the geodetic monuments (Langbein et al., 1995), which is of the order of 1 mm/yr$^{1/2}$ (Langbein and Johnson, 1997).

Table 1
Long Valley caldera leveling surveys

Year	Month(s)	Route(s)
1932	May–Oct	Hwy 395
1957	Aug–Nov	Hwy 395
1975	Jun–Aug	Hwy 395, Owens River Rd
1980	Oct	Hwy 395
1982	Aug–Nov	Complete
1983	Aug–Nov	Complete
1984	Jun–Aug	Complete
1985	Jun–Oct	Complete
1986	Jul–Oct	Complete
1987	Sep–Dec	Complete
1988	Oct–Nov	Complete
1992	Jul–Aug	Complete
1995	Jul–Aug	Hwy 395, Hwy 203
1997	Sep	Hwy 395, Hwy 203

Owens River Rd leveling route monitors deformation in the north moat and Long Valley plain (from station X123 to 8DOR through 24DO, 43DO and 48DO). Hwy 203 leveling route monitors the Mammoth Mt deformation (stations 2JCM and 5JCM).

4. Helmert orthometric heights

The first stage in the computation of the vertical deformation within Long Valley caldera is to reference the 1985 leveling survey to the NAVD88 vertical datum, by transforming the raw leveling heights into Helmert orthometric heights. The transformation is a two-step process: first, we compute the geopotential number associated with a leveling bench mark, then we calculate the Helmert height using the orthometric reduction formula (Heiskanen and Moritz, 1967, p. 167).

The geopotential number C_B represents the difference between the potential at the geoid and the potential at the observation point B (Heiskanen and Moritz, 1967, p. 162):

$$C_B = W_0 - W_B = \int_0^{h_B} g\,dh \qquad (1)$$

where 0 is a point at the mean sea level, that is on the geoid, h_B is the raw leveling height at B relative to 0, g is the external gravity (a function of the elevation h), and W is the gravitational potential. If A is the leveling survey datum (or primary base station) and B a second point on the leveling route, we have:

$$C_B = W_0 - W_B = (W_0 - W_A) + (W_A - W_B) =$$
$$C_A + \int_{h_A}^{h_B} g\,dh \qquad (2)$$

For normal orthometric heights, C_A is given by (Heiskanen and Moritz, 1967, p. 162):

$$C_A = \gamma_0 H^{dyn} \qquad (3)$$

where H^{dyn} is a local dynamic height expressed in the NAVD88 vertical datum, γ_0 is by convention the normal gravity value computed on the Geodetic Reference System ellipsoid of 1980 (GRS80) at 45° latitude. Dynamic heights scale the geopotential number by a global constant $\gamma_0 = 980.6199$ gal, converting the geopotential number into a length. The dynamic height for the bench mark C916 (the elevation datum for the Long Valley caldera leveling network) is $H^{dyn} = 2071.409$ m (see the data sheet for C916, PID = HR0097, available from the NGS server at http://www.ngs.noaa.gov/datasheet.html). To solve the integral in Eq. 2, we need values of the surface gravity g at every leveling bench mark between A and B. These values may be computed using the NAVD88 Modeled Gravity software, available from the NGS server at http://www.ngs.noaa.gov/TOOLS. Geopotential numbers are measured in g.p.u. (geopotential units), where 1 g.p.u. = 1 kgal m = 10 ms^{-2} m.

To compute the orthometric height at B, we substitute C_B into the Helmert's height reduction formula (Heiskanen and Moritz, 1967, p. 167):

$$H_B = \frac{C_B}{\overline{g}} = \frac{C_B}{g + 0.0424 H_B} \qquad (4)$$

where H_B is the orthometric height expressed in 10^3m and $\overline{g}$ is the mean value of the gravity along the plumb line between the geoid and the surface. If we use the simplified Prey reduction formula for the gravity, then $\overline{g} = g + 0.0424 H_B$ (Heiskanen and Moritz, 1967, p. 167), where g is the gravitational acceleration at B expressed in gal

Table 2
Horizontal deformation from 1985 to 1999 (two-color EDM data) Station coordinates in UTM (NAD27). Baseline change and error in m

Station	X	Y	Baseline	
			Change	Error
Common end point CASA				
CASA	332839.6	4167846.4	–	–
Hot	339457.6	4169286.4	0.170	0.005
Knol	325849.7	4169149.1	0.172	0.005
Krak	334429.6	4175494.2	0.336	0.005
Mine	331169.9	4164340.6	0.016	0.005
Shark	335777.9	4166871.7	0.062	0.005
Sher	328480.8	4165794.9	0.087	0.005
Till	335829.4	4164989.7	0.014	0.005
Common end point LKT				
LKT	328533.8	4177331.7	–	–
Bald	332747.8	4183347.3	0.049	0.005
Dead	322078.7	4177309.2	0.036	0.005
Knob	326622.4	4171597.5	0.204	0.005
Krak	334429.6	4175494.2	0.178	0.005
Mike	329323.1	4169648.8	0.287	0.005
Micr	325638.8	4181437.1	−0.014	0.005
Sage	337410.1	4178053.1	0.179	0.005

Horizontal deformation values have been averaged over the time span of the leveling and GPS survey. Leveling survey: June–October 1985. GPS survey: 13–31 July 1999.

(1 gal = 0.01 m/s^2). The approximated Eq. 4 is often sufficient for standard topography. Solving the algebraic Eq. 4, we get the value for the orthometric height at the leveling bench mark B:

$$H_B = \frac{-g + \sqrt{g^2 + 4 \times 0.0424 C_B}}{2 \times 0.0424} \qquad (5)$$

Orthometric heights for the 1985 leveling survey are shown in Table 3. The difference between the lowest (U123) and the highest (5JCM) leveled elevations is around 400 m. The standard errors for orthometric heights, taken to be the same as those of the leveled elevations (Zilkoski et al., 1992), range from 3 mm (station U123) to 24 mm (station F124) and average 20 mm within the caldera. Such relatively large errors are due to the long distance (40 km at the resurgent dome, 64 km at F124) between the leveling bench marks in the caldera and the base station C916 in Lee Vining.

5. GPS ellipsoidal heights

GPS phase and pseudorange observables were recorded on Trimble 4000 SSE and SSI receivers using Trimble Rugged L1/L2 with Ground Plane (TRM22020.00+GP) and Trimble 4000ST L1/L2 Geodetic (TRM14532.00) antennae. We recorded data for sessions that lasted about 8 h and frequently 12 h overnight. All sites were occupied for at least two sessions. In particular, the station C916 was occupied for 8-h sessions on six different days during the survey. Data from the USGS continuous GPS monitoring network were also included in the analysis.

We processed the GPS data with the Gipsy/Oasis II software (Lichten and Border, 1987), using a bias-fixed, fiducial-free, precise point positioning strategy (Zumberge et al., 1997). That is, we did not solve for the satellite orbits or clock errors, using instead solutions for these parameters provided by the Jet Propulsion Laboratory (JPL). The advantages to this approach include consistent realization of a standard reference frame, insensitivity to minor failures or data interruptions in the global tracking network, and computational efficiency. The primary disadvantage of this

strategy is that reference frame and orbital uncertainties are not propagated into the position covariance matrix.

Mixing different antenna types is known to degrade vertical precision; to mitigate this effect, we applied elevation-dependent phase center corrections (Rothacher et al., 1996) from the International GPS Service (IGS) during the processing.

Because the primary aim of this survey was vertical precision, we used a very low elevation mask of 5°. A mask of 15° is more commonly used, since tropospheric path delays below that angle cannot be modeled easily. To circumvent this problem, we modeled tropospheric gradients (see Bar-Sever et al., 1998), to permit azimuthal variations in path delay in addition to the standard elevation dependency. Thus, we solved for three tropospheric parameters per station per data epoch: the perturbation on the nominal total zenith delay, and the two components of the tropospheric gradient. All the tropospheric parameters were modeled stochastically, using a random walk with a scale of 50 mm/day$^{1/2}$ for the zenith delay, and a scale of 1.5 mm/day$^{1/2}$ for the gradient components. Because of the altitude (the average elevation of Long Valley caldera is approximately 2500 m), the wet zenith delay is significantly smaller than at sea level.

We used the parameters for a Helmert transformation provided by JPL to transform each daily solution into the ITRF96 reference frame. We transformed the ITRF96 XYZ solutions into geodetic latitude, longitude and ellipsoidal heights using the NAD83 ellipsoidal model for the continental United States and the Horizontal Time-Dependent Positioning (HTDP) software (available from the NGS server at http://www.ngs.noaa.gov/TOOLS). GPS ellipsoid heights and their uncertainties for the 1999 survey are reported in Table 3. The 1σ uncertainties for the GPS point positions were derived by scaling the formal errors by the square root of chi-square per degree of freedom of the daily solutions for station C916 (the dimensionless scale factor is 3.68). Uncertainties in the GPS ellipsoidal heights range from 6 mm (station C916) to 66 mm (station MUSE) and average 18 mm. Four stations (W911, MUSE, 5JCM and 16EGE) have uncer-

Table 3
Vertical deformation by comparing GPS and leveling

	X	Y	1985 heights[a]		1999 GPS heights[b]		GEOID heights[c]		Uplift	
			Elev. (m)	± (m)	Elev. (m)	± (m)	Elev. (m)	± (m)	(m)	± (m)
C916	315132.0	4201661.4	2073.911	0.000	2049.515	0.006	−24.403	0.044	0.007	0.044
U123	315350.0	4200413.0	2067.752	0.003	2043.348	0.010	−24.401	0.043	−0.002	0.044
X123	326127.3	4178629.4	2281.845	0.016	2257.308	0.009	−24.697	0.036	0.160	0.040
B13	327780.1	4175875.0	2333.646	0.017	2308.958	0.040	−24.824	0.036	0.137	0.056
D916	328094.6	4174458.6	2313.526	0.017	2288.899	0.012	−24.844	0.036	0.217	0.041
13DOR	329091.7	4172772.8	2312.050	0.018	2287.431	0.008	−24.872	0.035	0.253	0.040
12DOR	329558.8	4171897.3	2312.341	0.018	2287.727	0.010	−24.878	0.035	0.264	0.041
W911	330131.2	4169698.7	2243.825	0.019	2219.252	0.057	−24.859	0.035	0.286	0.069
8DOR	339179.7	4164855.8	2146.746	0.021	2122.068	0.011	−24.846	0.037	0.168	0.044
CONV	340248.2	4164402.2	2152.286	0.021	2127.591	0.011	−24.843	0.037	0.147	0.044
7DOR	340789.5	4163159.7	2100.840	0.022	2076.208	0.015	−24.773	0.037	0.141	0.045
V911	341581.1	4162067.9	2088.615	0.022	2064.04	0.017	−24.727	0.037	0.152	0.046
U911	343683.4	4160673.9	2110.122	0.022	2085.548	0.009	−24.682	0.038	0.108	0.045
D124	344672.2	4159700.7	2114.061	0.023	2089.511	0.016	−24.678	0.038	0.128	0.047
E124	347629.5	4158613.7	2198.150	0.024	2173.517	0.012	−24.731	0.039	0.099	0.047
F124	350192.9	4158178.5	2135.976	0.024	2111.296	0.013	−24.806	0.040	0.127	0.048
2JCM	328808.7	4167628.0	2333.308	0.020	2308.765	0.011	−24.774	0.035	0.231	0.042
5JCM	324333.7	4169320.3	2506.505	0.021	2481.938	0.051	−24.754	0.035	0.187	0.065
13JCM	331087.8	4175906.6	2265.732	0.019	2241.069	0.018	−24.896	0.036	0.233	0.045
15JCM	332778.6	4174484.5	2326.528	0.020	2301.811	0.010	−24.957	0.036	0.240	0.042
9PDI	333400.2	4173817.1	2268.263	0.020	2243.568	0.021	−24.963	0.036	0.268	0.046
11PDI	333872.8	4173197.0	2238.038	0.020	2213.345	0.013	−24.964	0.036	0.271	0.043
17JCM	333626.2	4171903.2	2244.412	0.021	2219.786	0.026	−24.954	0.036	0.328	0.049
25EGE	333591.8	4171071.4	2302.406	0.021	2277.74	0.012	−24.948	0.036	0.282	0.043
23EGE	332686.5	4171245.1	2344.610	0.021	2319.961	0.013	−24.943	0.036	0.294	0.043
18EGE	331855.0	4170274.0	2328.933	0.022	2304.352	0.024	−24.909	0.035	0.329	0.048
16EGE	331550.1	4169603.1	2308.368	0.022	2283.818	0.060	−24.885	0.035	0.335	0.073
14EGE	331126.0	4169145.5	2277.955	0.022	2253.307	0.029	−24.865	0.035	0.217	0.051
MUSE	328750.3	4178852.1	2229.557	0.018	2205.001	0.066	−24.766	0.036	0.210	0.077
E916	329965.2	4179626.2	2229.731	0.018	2205.144	0.027	−24.755	0.037	0.168	0.049
G916	333533.7	4179120.4	2163.660	0.019	2138.989	0.014	−24.828	0.037	0.157	0.044
24DOR	336425.1	4178685.1	2132.931	0.020	2108.16	0.008	−24.874	0.038	0.102	0.043
39DOR	340129.9	4176536.7	2112.372	0.021	2087.447	0.006	−24.997	0.038	0.072	0.044
41DOR	340379.8	4173956.7	2099.015	0.022	2074.088	0.009	−25.053	0.038	0.126	0.044
43DOR	340344.2	4172114.8	2113.214	0.022	2088.266	0.008	−25.058	0.037	0.110	0.044
45DOR	340212.0	4170297.0	2127.682	0.022	2102.796	0.010	−25.042	0.037	0.156	0.044
46DOR	340780.9	4169142.7	2124.423	0.023	2099.522	0.014	−25.032	0.037	0.131	0.046
47DOR	340417.2	4168128.5	2137.045	0.023	2112.18	0.010	−25.006	0.037	0.141	0.045
48DOR	340225.1	4166866.8	2127.544	0.023	2102.718	0.013	−24.963	0.037	0.138	0.046
1JD	340232.1	4166311.7	2129.720	0.023	2104.92	0.011	−24.940	0.037	0.140	0.045
26JCM	337626.7	4172101.1	2158.560	0.022	2133.766	0.008	−25.016	0.037	0.222	0.043
49DOR	341431.8	4172249.2	2119.059	0.022	2094.062	0.006	−25.065	0.038	0.068	0.044
50DOR	343685.1	4172450.5	2081.868	0.023	2056.845	0.010	−25.067	0.038	0.044	0.046
4JD	344662.3	4173752.9	2079.315	0.023	2054.315	0.010	−25.043	0.039	0.044	0.046

Bench mark coordinates in UTM (NAD27).

[a] Leveled orthometric heights (NAVD88).

[b] GPS ellipsoid heights (NAD83).

[c] Locally corrected geoid model.

tainties between 51 and 66 mm because of poor sky visibility (see Table 3).

6. GPS-based orthometric heights

Eq. 6 gives the general relationship between ellipsoid heights (heights between the external surface and the ellipsoid), h, orthometric heights (heights between the external surface and the geoid), H, and geoid height (distance between the ellipsoid and the geoid), N (see Fig. 5):

$$h = H + N \qquad (6)$$

In the United States the geoid surface is beneath the ellipsoid. Thus, geoid heights N are negative, and the ellipsoidal height h is smaller in magnitude than the orthometric height H at a given point. Subtracting the geoid heights N from the ellipsoid heights h, we can obtain GPS-based orthometric heights H (Milbert and Smith, 1996).

Gravity points, digital elevations and altimetrically derived gravity anomalies can be processed to compute a geocentric gravimetric geoid height model (Milbert, 1991; Smith and Milbert, 1999). Unfortunately, we cannot directly transform between NAD83 GPS ellipsoid heights and NAVD88 orthometric heights using a gravimetric geoid. The reason is that there is a systematic offset between the NAVD88 reference level and the current best estimate of global mean sea level, while a transcontinental tilt is introduced by the non-geocentricity of the NAD83 ellipsoid (Smith and Milbert, 1999). To transform directly between GPS ellipsoid heights and orthometric heights, we need to relate the geoid height N, the ellipsoidal heights h and the orthometric heights H through an empirical conversion surface s (Milbert, 1995; Kotsakis and Sideris, 1999). If subscripts are used to denote the height reference systems, then we can rewrite Eq. 6 as:

$$H_{88} = h_{83} - (N + s) \qquad (7)$$

where H_{88} indicates the GPS-based orthometric heights relative to NAVD88, and h_{83} the GPS ellipsoid heights relative to NAD83. The new geoid model $N+s$ is called a hybrid geoid (Smith and Milbert, 1999). The NGS released the latest gravimetric geoid model (G99SSS) and hybrid geoid model (GEOID99) for the continental United States in 1999 (Smith and Roman, 1999).

GPS-based orthometric heights may be compared with existing leveled orthometric heights to check the relative accuracy of the geoid model in the area. Unfortunately, no bench marks were occupied at the same time by leveling and GPS in Long Valley, because the USGS conducted GPS and leveling surveys in alternate years (i.e. we have GPS surveys in 1994, 1996 and 1998, and leveling in 1995 and 1997). So, we decided to qualitatively check the accuracy of the geoid model by comparing the uplift along Hwy 395 measured by differencing orthometric heights from the 1975 and 1997 leveling surveys, with the uplift measured by differencing the 1999 GPS-based orthometric heights and the 1975 leveled orthometric heights. We expect the 1999–1975 uplift to exceed the 1997–1975 uplift, given the strong activity registered in the caldera between the fall of 1997 and the spring of 1998 (Fig. 3). Using the horizontal deformation along the CASA–KRAK baseline as a proxy for the uplift, we would expect a vertical deformation at the resurgent dome of about 8.5 cm between September 1997 and July 1999 (Fig. 4). Results from our qualitative check are shown in Fig. 6. We can see that while the pattern of the deformation is the same (Fig. 6b), the 1999–1975 uplift is actually smaller than the 1997–1975 uplift (Fig. 6c). In particular, we have a subsidence of -2 ± 6 cm at the resurgent dome (bench mark W911) in the 1997–1999 interval. We know from EDM measurements of the deformation in Long Valley caldera (Figs. 3 and 4) that no major episode of contraction (and therefore subsidence) of the resurgent dome took place between 1997 and 1999. Our interpretation is that the GEOID99 model is globally accurate, but requires a local adjustment (Smith and Roman, 1999), probably because the NGS used only four points to estimate the conversion surface s in the Long Valley area (Table 4).

According to Milbert and Smith (1996), to model the conversion surface s, first we have to form the residuals e at collocated sites:
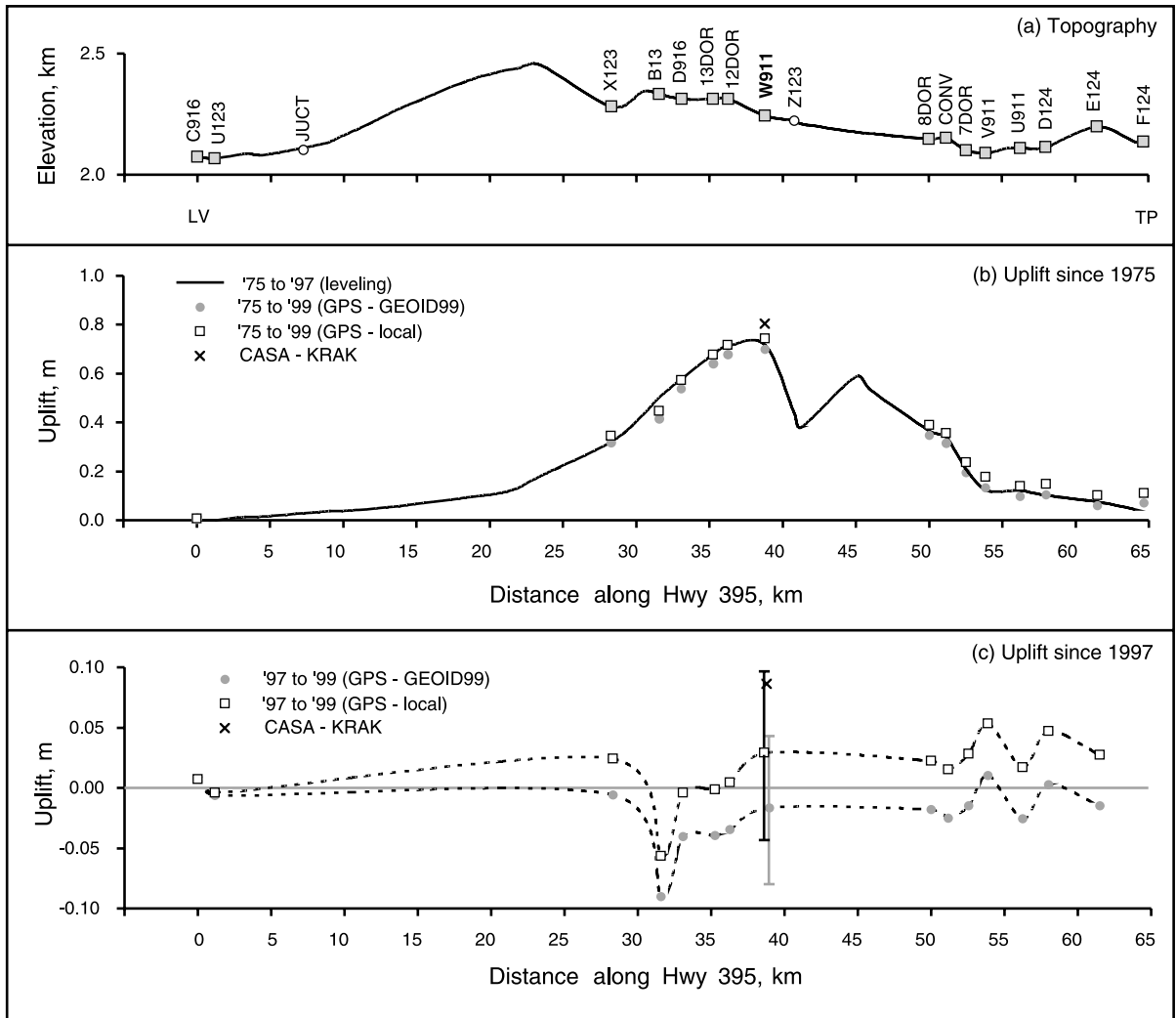
Fig. 6. Qualitative check of the GEOID99 geoid height model in Long Valley. (a) Topography along Hwy 395 leveling route. The bench marks correspond to those leveled in 1975 and occupied with GPS in 1999. LV: Lee Vining; TP: Tom's Place. (b and c) Deformation profiles along Hwy 395 leveling route. The GPS (GEOID99) label indicates GPS-based orthometric heights computed using the NGS GEOID99 geoid height model. GPS-local refers to correction with the 'locally corrected' conversion surface derived here. CASA–KRAK denotes the uplift (8.5 cm) expected at W911 using the horizontal deformation along the CASA–KKRAK two-color baseline as a qualitative estimate for the expected uplift (see Fig. 4). The uplift measured at W911 since 1997 is -2 ± 6 cm using GEOID99 and 3 ± 7 cm using the local conversion surface. Error bars (1σ) shown for clarity only at W911.

$$e = h_{83} - N - H_{88} \qquad (8)$$

To improve the estimate of the conversion surface s in Long Valley, we need to increase the number of co-located GPS and leveling bench marks used in the computation. Given that no GPS and leveling surveys were run in Long Valley

in the same year, the best possible compromise is to use the 1994 GPS survey and the 1995 leveling survey. The NGS occupied four leveling bench marks with GPS in 1991; the USGS occupied five leveling bench marks with GPS in 1994 (Table 4). One of these bench marks (JUCT) is common to the USGS and NGS data set, so we have

a total of eight points with co-located GPS and leveling measurements (Fig. 7). We must, however, bound the vertical motion during the 1994–1995 period. Using leveling data from the 1992 and 1995 survey, the uplift predicted at most of the collocated data points from 1994 to 1995 (assuming a constant deformation rate) is no greater than 1 cm, and is not significant at 95% confidence level (Table 4). Two-color EDM data confirm that the deformation rate was nearly constant during the 1992–1995 interval (Fig. 3; Fig. 4), so this interpolation should be reasonable. If e is significantly greater than the predicted uplift (see Table 4), we can assume that e approximates the value of the conversion surface s at the collocated bench mark. This assumption is valid for two points of the NGS data set (E818 and L1408) and five points of the USGS data set (U123, JUCT, Z123, CONV and RET); we reject one point of the NGS data set (X123), because the predicted uplift is greater than the residual (Table 4).

To compute the 'locally corrected' conversion surface s, we fit a planar surface:

$$s = m_1 + m_2 x + m_3 y \qquad (9)$$

to the residuals e, using weighted least squares to estimate the parameters:

$$m_1 = -0.1409 \pm 0.0344 \text{ m};$$

$$m_2 = 0.0025 \pm 0.0007 \text{ m/km};$$

$$m_3 = 0.0013 \pm 0.0007 \text{ m/km} \qquad (10)$$

We compute the new 'locally corrected' hybrid geoid height at each GPS bench mark (see Table 3) by adding s, given by Eqs. 9 and 10, to the NGS gravimetric geoid G99SSS (Smith and Roman, 1999). The stated uncertainties in the 'locally corrected' hybrid geoid model are from the propagation of errors from Eqs. 9 and 10 only, because there is no formal accuracy estimate for the gravimetric geoid G99SSS (Roman, NGS, personal communication). Geoid uncertainties range from 35 to 44 mm, and average 37 mm. The qualitative check of the new 'locally corrected' geoid height model shows an improvement in the estimate of the vertical deformation. The 1975–1999 uplift is now greater than the 1975–1997 uplift (Fig. 6b). The measured vertical deformation between 1997 and 1999 at the resurgent dome (bench mark W911) is now 3 ± 7 cm, a val-

Table 4

Co-located GPS and leveling bench marks used to model the conversion surface s in Long Valley

Bm ID	h_{83}	N	H_{88}	e	Predicted uplift[d]
NGS data[a]					
E818	1732.688	−24.915	1757.546	0.057	–
JUCT	2078.911	−24.278	2103.311	−0.122	0.009 ± 0.009
X123[b]	2257.233	−24.592	2281.86	−0.035	0.041 ± 0.017
L1408	1183.871	−26.215	1210.058	0.028	–
USGS data[c]					
U123	2043.375	−24.297	2067.752	−0.080	-0.001 ± 0.002
JUCT	2078.946	−24.278	2103.328	−0.104	0.000 ± 0.004
Z123	2198.817	−24.723	2223.662	−0.122	-0.009 ± 0.009
CONV	2127.547	−24.755	2152.399	−0.097	0.013 ± 0.010
RET	2800.608	−24.546	2825.211	−0.057	0.010 ± 0.011

N is the gravimetric geoid G99SSS, h_{83} the GPS heights, and H_{88} the leveled heights, e the residuals. All data are in m. Errors correspond to one standard deviation.

[a] NGS data: GPS heights measured in 1991; leveled heights in the summer of 1988.

[b] The bench mark X123 has not been included in the modeling of the conversion surface s, because the deformation at this point (4.1 ± 2.3) is significant.

[c] USGS data: GPS heights are from the 1994 survey, while leveled heights are from the 1995 survey.

[d] Deformation at the NGS data points estimated using the average deformation rate from the 1988 and 1992 leveling surveys. Deformation at the USGS data points estimated using the average deformation rate between 1992 and 1995.
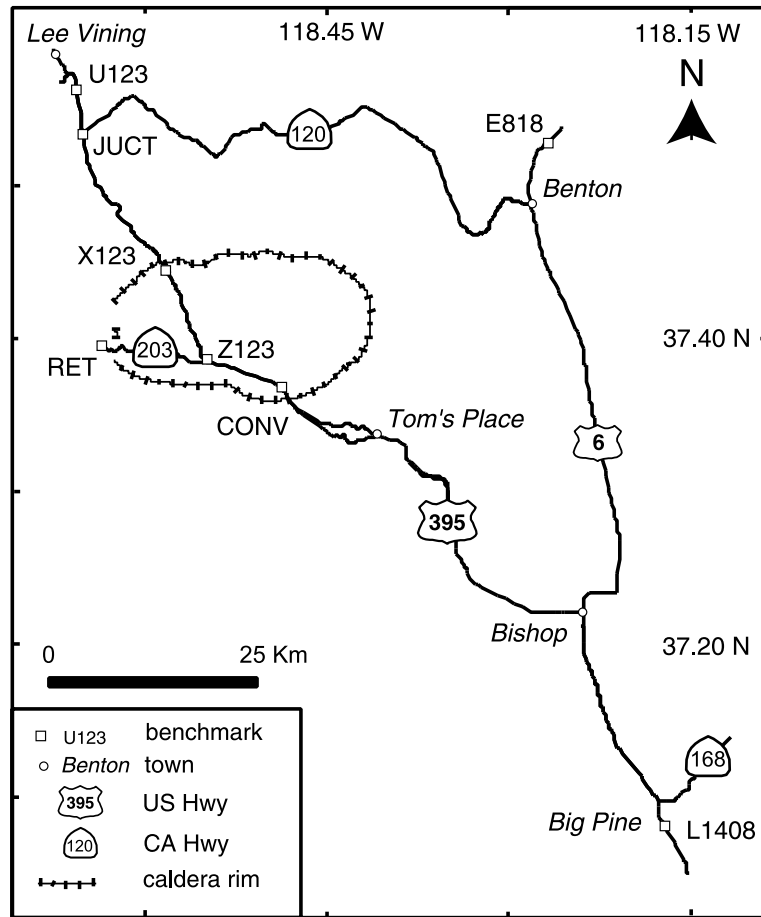
Fig. 7. Co-located GPS and leveling bench marks used to model the local conversion surface *s* in Long Valley (see Table 4).

ue within one standard deviation of the 8.5 cm of uplift inferred from the change in the CASA–KRAK baseline length (see Fig. 4).

The development of the uplift from 1975 to 1999 along Hwy 395 and Owens River Rd is shown in Fig. 8. Uncertainties in the uplift range from 40 mm (station 12DOR) to 77 mm (station MUSE) and average 47 mm. Errors in the 'locally corrected' geoid dominate our estimate of the uplift, accounting for about 2/3 of the total error.

7. Modeling the inflation source

We model the inflation source by inverting both vertical and horizontal displacements for either a spherical or ellipsoidal source in an elastic, homogeneous, isotropic half-space (Fig. 9). The spherical source is a well known and widely used standard to model the deformation of the Earth's crust due to the inflation of a magma body (e.g. McTigue, 1987). If the radius of the inflating spherical source is smaller than its depth, a point source approximation works well (McTigue, 1987):

$$U_z = (1-\nu)\frac{\Delta V}{\pi}\frac{d}{R^3} \qquad (11)$$

$$U_r = (1-\nu)\frac{\Delta V}{\pi}\frac{r}{R^3} \qquad (12)$$

where U_z and U_r are the vertical and horizontal displacement, ν is the Poisson's ratio,
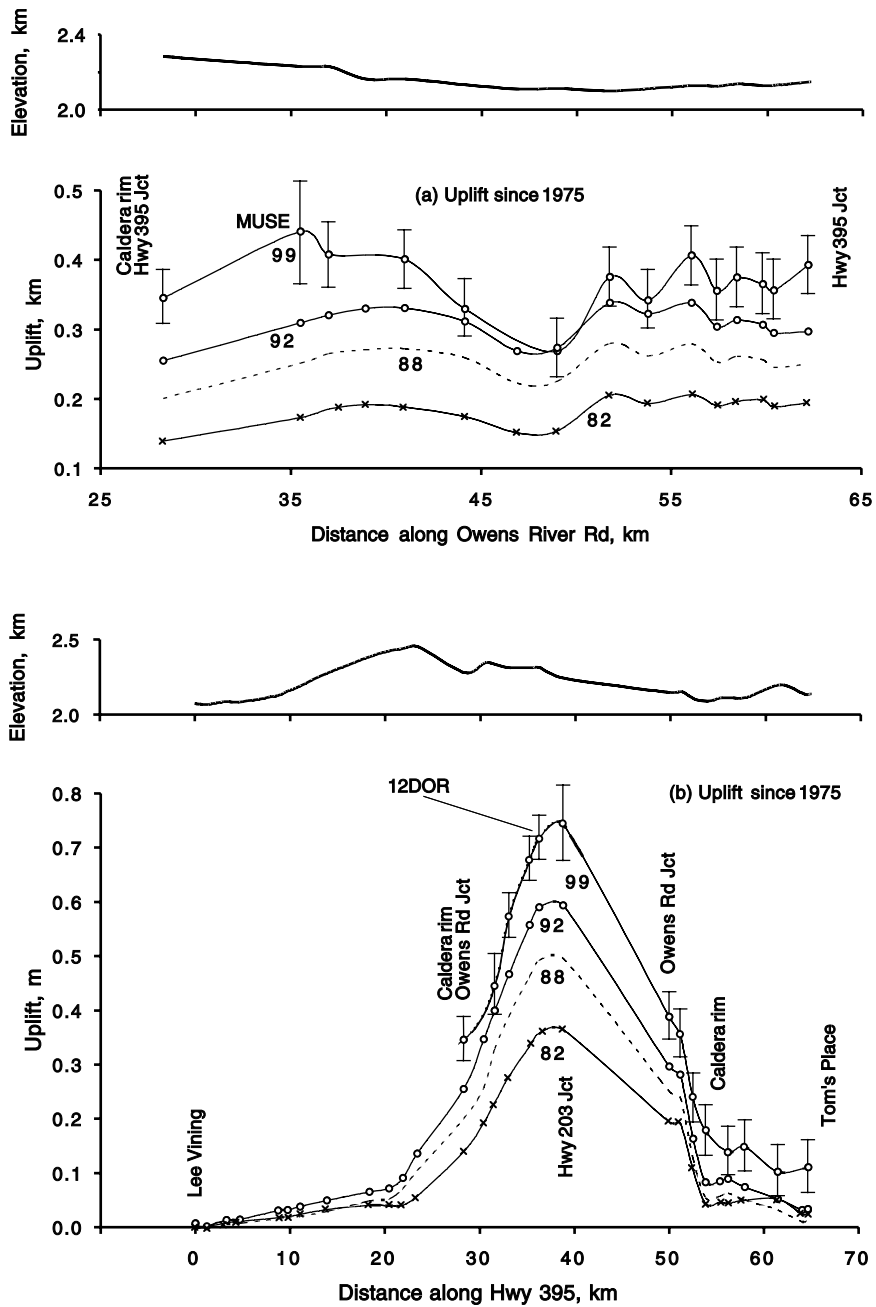
Fig. 8. Uplift profiles relative to 1975 from leveling surveys in 1982, 1988, 1992 and 1999 along Hwy 395 and Owens River Rd. Owens River Rd is the leveling route around the resurgent dome from station X123 to station 8DOR. Topographic profiles along the routes are shown at the top. 1σ error bars shown only for the 1975–1999 uplift.
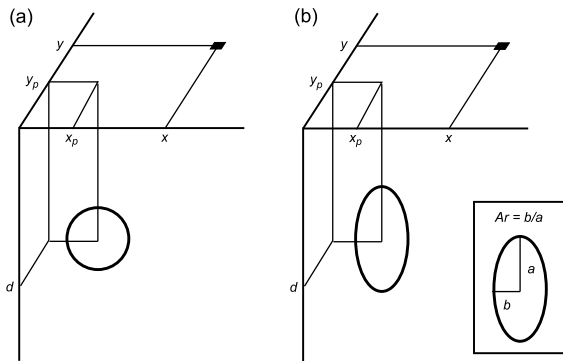
Fig. 9. Source geometry: (a) spherical model; (b) ellipsoidal model. The assumed parameters for the ellipsoidal model are $a = 1$ km, dip angle $= 90°$, orientation angle $= 0°$.

$r = \sqrt{(x-x_{\mathrm{p}})^2 + (y-y_{\mathrm{p}})^2}$ is the radial distance from the surface projection of the center of the sphere at $(x_{\mathrm{p}}, y_{\mathrm{p}})$, to the bench mark at (x,y), d is the depth of the center of the sphere from the surface, $R^2 = r^2 + d^2$, and ΔV is the volume change of the inflating sphere. Despite its simplicity, the point source model often represents surface uplift quite well (e.g. Nishi et al., 1999). To model the inflation of a vertically elongated magma body, Yang et al. (1988) derived analytic expressions for the deformation field due to the inflation of a finite, prolate ellipsoidal source. The resulting equations for the horizontal and vertical deformation are a function of the pressure change ΔP, the ellipsoid geometry (semi-major axis a and semi-minor axis b), the location (x_{p}, y_{p} and the depth d), and the orientation of the ellipsoid (dip and dip orientation). The volume change ΔV induced by a pressure change ΔP within an ellipsoidal cavity far from the free surface is (Tiampo et al., 2000):

$$\Delta V = \frac{\Delta P}{\mu}\pi a b^2 \tag{13}$$

where μ is the shear modulus of the elastic half-space. We assume that the major axis a of the ellipsoid is vertical for simplicity and normalized to 1 km, because the deformation is insensitive to the magnitude of a as long as the major axis of the inflating ellipsoid is somewhat smaller than its depth (see Table 5).

To invert the data, we employ a grid search algorithm that specifies the location (xp, yp and d) and geometry (b/a) of the inflation source to compute the vertical and horizontal displacements due to a unit volume change at every data point. For each choice of geometrical parameters, we use weighted least squares to estimate the volume change. The source model with the smallest χ^2 is selected:

$$\chi^2 = \delta^T \Sigma^{-1}\delta \tag{14}$$

where δ is the difference between the observed and predicted displacements, and Σ the data covariance matrix. The proportion of variability of the observed data explained by a given source model is:

$$R^2 = 1 - \frac{\delta^T \Sigma^{-1}\delta}{U^T \Sigma^{-1} U} \tag{15}$$

where U are the observed displacements. If $R^2 = 1$, then the model is able to explain all variation in the observed data; if $R^2 = 0$, the model is not able to explain the observed data.

We start by fitting a spherical source to the vertical and horizontal displacements (Fig. 10). Although this source, located 8 km beneath the resurgent dome, explains approximately 98% of the two-color data (Fig. 10), we find that the fit to vertical deformation is poor, with only 8% of uplift data explained by the model (Fig. 11; Table 6). In particular, the model overestimates the deformation at the resurgent dome, and underestimates the deformation south of the caldera. The fit of an ellipsoidal source to the deformation data (Figs. 12 and 13) significantly reduces the size of the residuals in the leveling data, while only

Table 5
Inversion results for an ellipsoidal source

a	d	ΔV	χ^2		R^2	
(km)	(km)	(km^3)	Uplift	EDM	Uplift	EDM
0.25	5.9	0.087	67	271	0.73	0.98
0.5	5.9	0.087	67	270	0.73	0.98
1	5.9	0.086	67	267	0.73	0.98
2	6.1	0.089	67	256	0.73	0.98
4	6.9	0.102	70	224	0.72	0.98

The aspect ratio (b/a) and position of the source are those of the best fit ellipsoid model defined in Table 6. EDM labels the horizontal displacements.
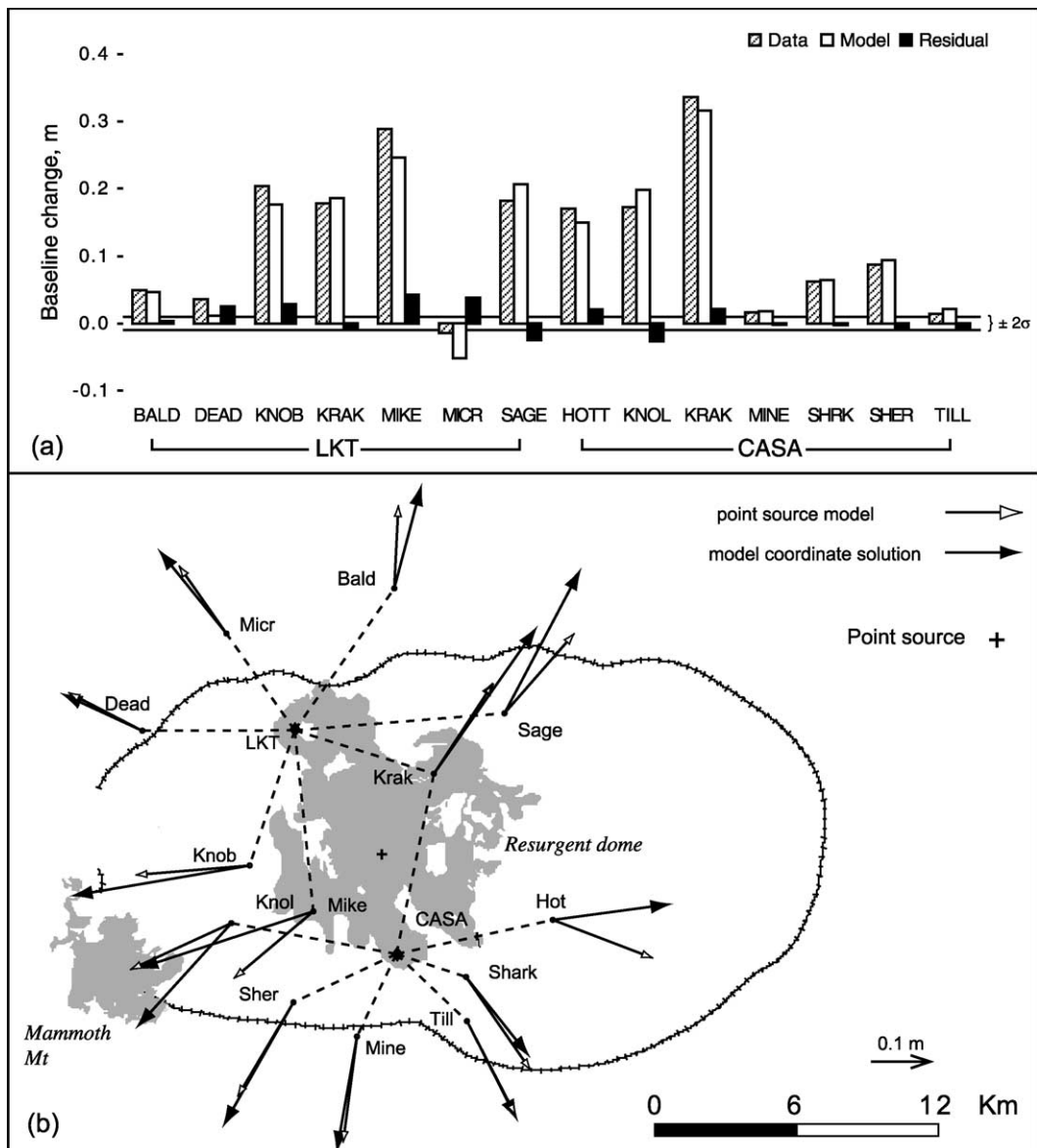
Fig. 10. Optimal spherical source (depth = 8 km, volume = 0.124 km³). (a) Observed and predicted baseline changes ($\chi^2 = 239$; $R^2 = 0.98$); (b) model coordinate solution (Segall and Matthews, 1988) for displacements in the two-color EDM network, using displacements predicted by the spherical source model. Displacement errors (~ 5 mm) are too small to be drawn.

slightly increasing the misfit to the two-color data (Table 6). The ellipsoidal source is located 5.9 km beneath the resurgent dome, has an aspect ratio $b/a = 0.475$, and is able to explain 98% of the two-color data (Fig. 12) and 73% of the uplift data (Fig. 13). It is worth noting that the most significant discrepancy between predicted and observed

uplift is at bench marks farthest from the primary base station C916, where the cumulative effects of small systematic errors are likely to be greatest. In summary, the ellipsoidal model clearly provides a better fit to the observed horizontal and vertical deformation than the spherical model.

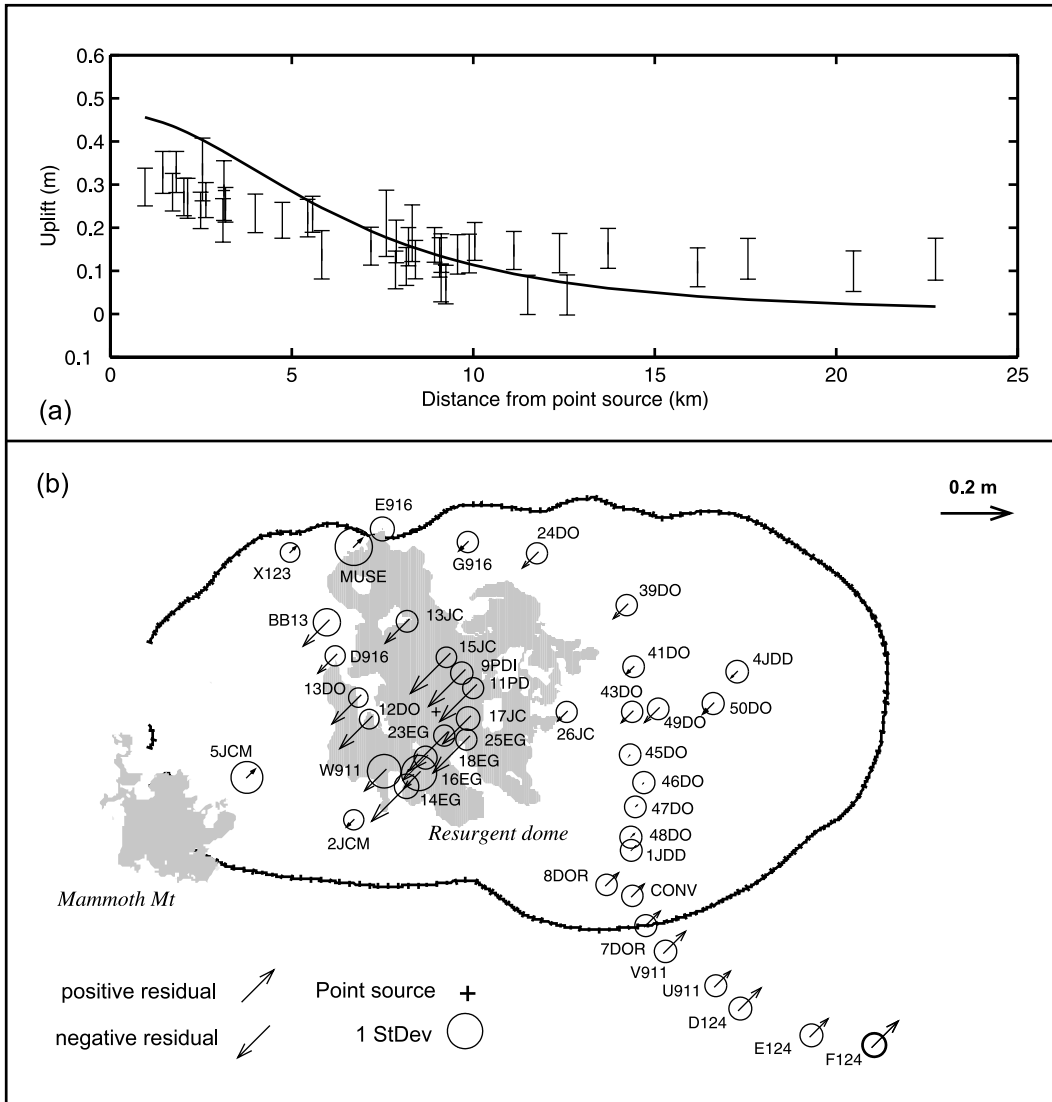We employed a bootstrap percentile method to

Fig. 11. Optimal spherical source (depth = 8 km, volume = 0.124 km^3). (a) Comparison between observed (error bars) and predicted (solid line) uplift ($\chi^2 = 228$; $R^2 = 0.08$). (b) Residual distribution (observed–predicted uplift).

Table 6
Best fit inflation source

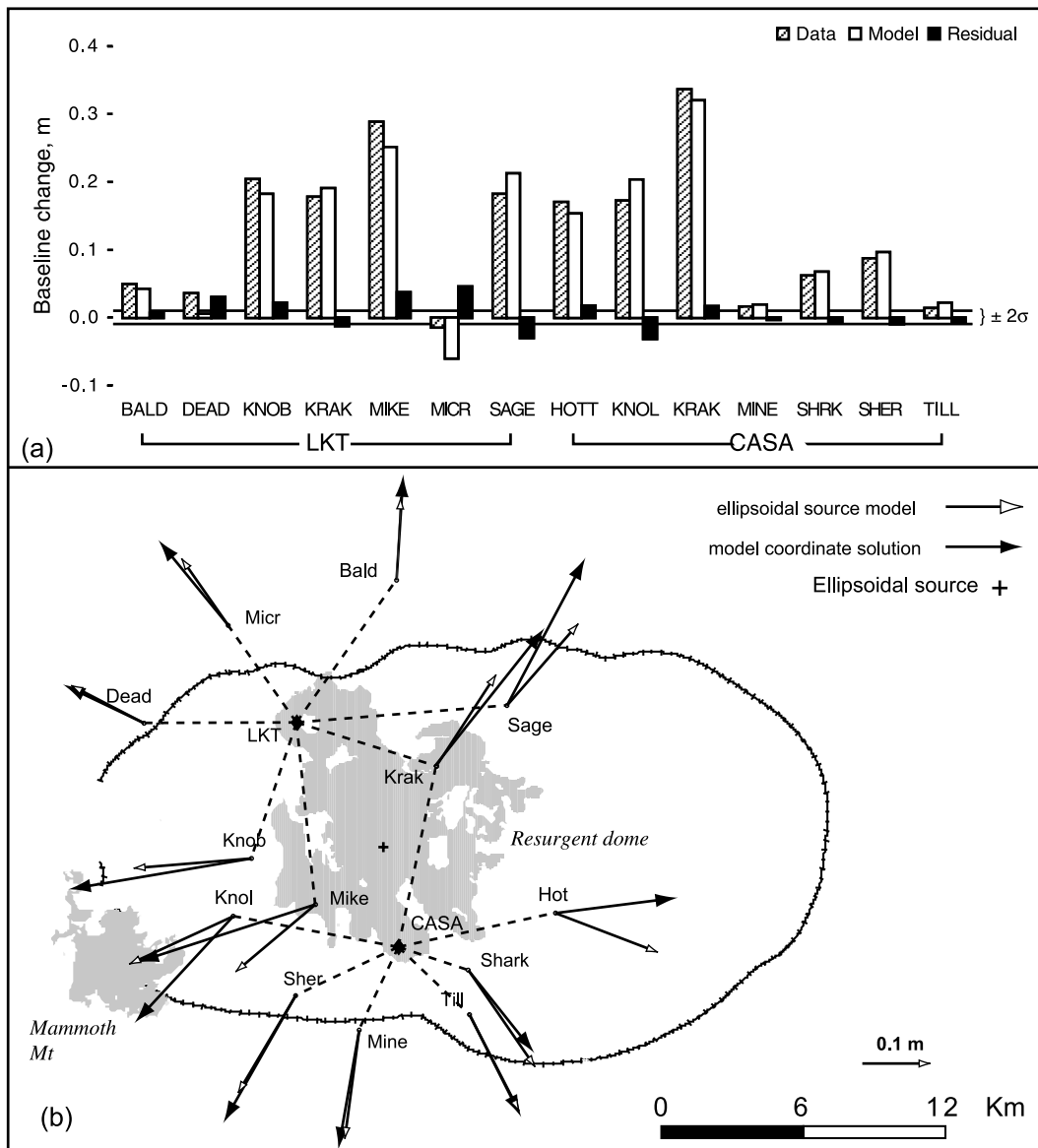|	b/a	x_p (UTM)	y_p (UTM)	d (km)	ΔV (km^3)	χ^2 Uplift	Two-color	Both	R^2 Uplift	Two-color
Spherical	1	322188	4172064	8	0.124	228	239	467	0.08	0.98
Ellipsoidal	0.475	322188	4172064	5.9	0.086	67	267	334	0.73	0.98

Position in UTM (NAD27) coordinates.

Fig. 12. Optimal ellipsoidal source (depth = 5.9 km, volume = 0.0.086 km³, b/a = 0.475). (a) Observed and predicted baseline changes (χ^2 = 267; R^2 = 0.98); (b) model coordinate solution (Segall and Matthews, 1988) for displacements in the two-color EDM network, using displacements predicted by the ellipsoidal source model. Displacement errors ($\sim$5 mm) are too small to be drawn.

obtain 95% confidence bounds on the parameters of the ellipsoidal model (Efron and Tibshirani, 1986). With the bootstrap, the data set is randomly resampled with replacement (i.e. some stations appear multiple times, others not at all). The resampled data set is inverted for source geometry, depth and volume, and the process is repeated 1000 times. 95% confidence intervals are determined by ordering the bootstrap results and excluding the smallest and largest 2.5% of the dis-

tribution. The method yields a 95% bound on depth of 4.9–7.6 km, 0.25–0.65 on the aspect ratio (*b/a*), and 0.06–0.13 km^3 on the volume change.

8. Summary and conclusions

Our work shows that GPS may achieve a precision similar to second-order leveling on distance scales appropriate to monitoring caldera wide deformation. The average height uncertainty in our data set is 20 mm for leveling and 18 mm for GPS. The largest contribution to the uncertainty in the uplift comes from the error in the geoid height model, not from leveling or GPS elevations (Fig. 14). We have been able to tie GPS and leveling to a common reference frame in the Long Valley area, and compute the vertical deformation by differencing GPS-based and leveled orthometric heights. The resurgent dome uplifted roughly 74 cm from 1975 to 1999 (74 ± 7 cm at the leveling station W911).
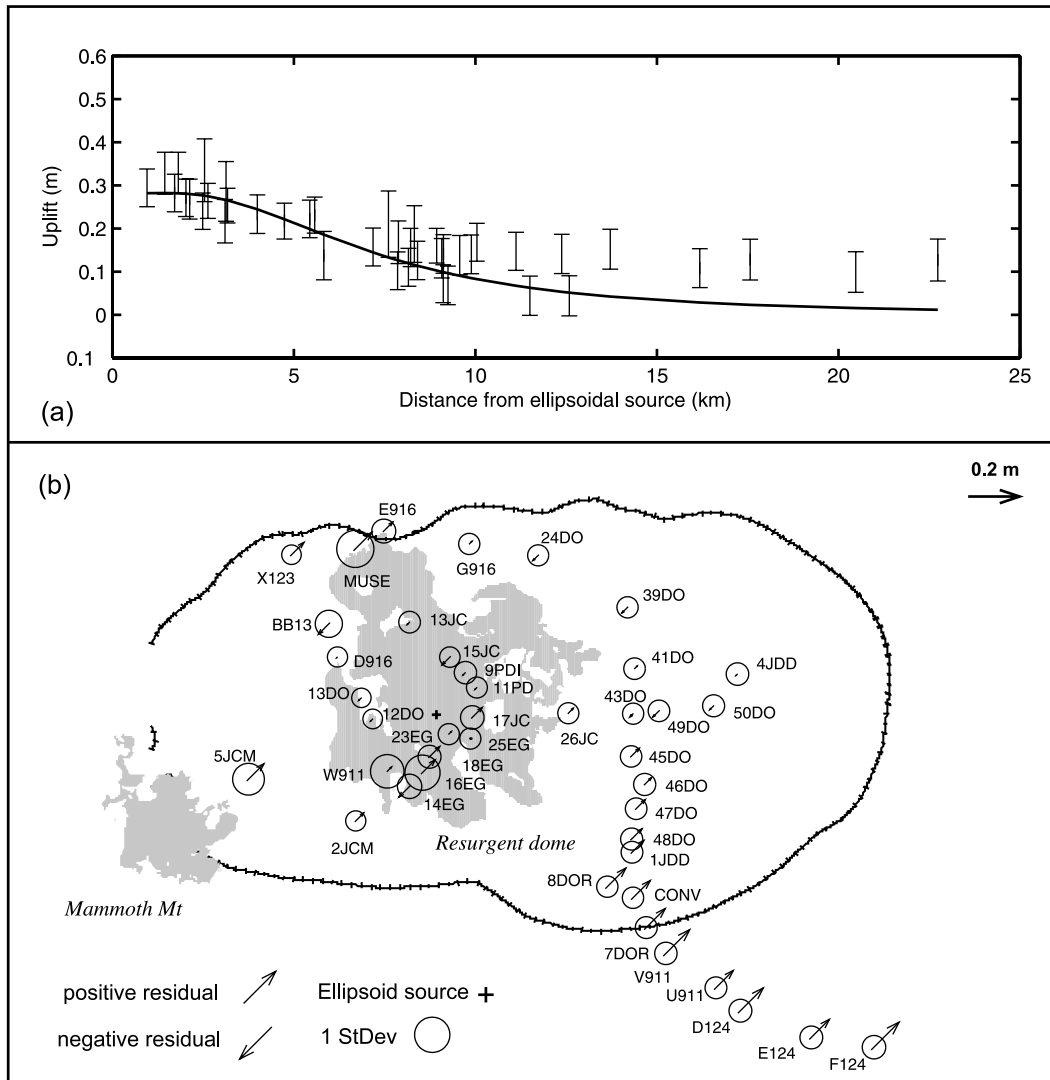

Fig. 13. Optimal ellipsoidal source (depth = 5.9 km, volume = 0.086 km^3, *b/a* = 0.475). (a) Comparison between observed (error bars) and predicted (solid line) uplift (χ^2 = 67; R^2 = 0.73). (b) Residual distribution (observed–predicted uplift).
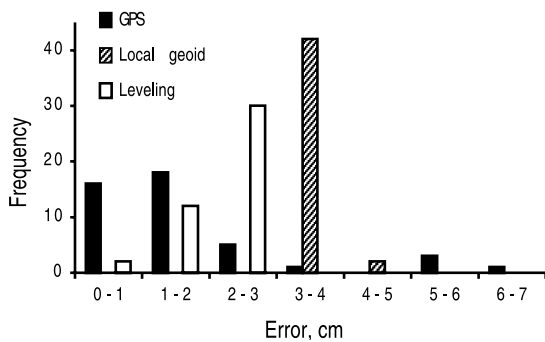
Fig. 14. Error distribution (one standard deviation) for GPS, geoid and leveling heights. The average standard error is 18 mm for GPS, 20 mm for leveling and 37 mm for the local geoid. Errors in the geoid dominate our estimate of the uplift, accounting for about 2/3 of the total error.

The inflation of the resurgent dome is the most prominent feature of the caldera deformation field. To define the inflation source, we invert two-color and uplift data from the 1985–1999 unrest period (Tables 2 and 3) using both a spherical and an ellipsoidal model. The ellipsoidal source satisfies both the vertical and horizontal deformation data, whereas the spherical point source does not. Whereas both models are able to explain about 98% of the observed two-color data, the spherical source fits the uplift poorly, when compared with the ellipsoidal model (Table 6). It is not clear if the observed discrepancy between predicted and observed uplift south of the caldera

rim (Figs. 11 and 13) is simply an artifact introduced by measurements or geoid errors, or due to deformation related to seismic activity along the Hilton Creek and Round Valley faults in the Sierra Nevada (e.g. Kahle et al., 1986). According to our analysis, the main intrusive body is located beneath the resurgent dome at a depth of 5.9 km (95% bounds of 4.9–7.5 km). This body has an aspect ratio of 0.475 (95% bounds are 0.25–0.65) and a volume change (from 1985 to 1999) of 0.086 km³ (95% bounds are 0.06–0.13 km³). The inversion results are independent of the finite dimensions of the ellipsoid, as long as the major axis of the inflating ellipsoid is substantially smaller than its depth (Table 5).

The type of model used to invert the data may bias the depth and volume of the inflation source beneath the resurgent dome. Comparing several existing studies of the caldera deformation source, we can see that spherical models systematically yield a deeper inflation source than ellipsoidal models (Table 7). Spherical models position the deformation source beneath the resurgent dome at about 7–12 km, whereas ellipsoidal sources locate the source at about 5.5–7 km. A similar comparison for volume change is not possible, because the models reviewed do not span the same deformation interval (Table 7).

Our results confirm the existence of a shallow source of inflation beneath the resurgent dome (e.g. Langbein et al., 1995), but do not exclude

Table 7
Estimated depths of the inflation source beneath the resurgent dome

Paper	Geodetic data	Interval	Best fit model	
			depth (km)	source
Estrem et al. (1985)	trilateration	1983–1984	10	spherical
Savage et al. (1987)	leveling, trilateration	1982–1986	10	spherical
Wu and Wang (1988)	leveling, trilateration	1975–1982	9.5	spherical
Langbein et al. (1989)	two-color EDM	1983–1988	10	spherical
Langbein et al. (1993)	two-color EDM	1989–1991	7	spherical
Langbein et al. (1995)	two-color EDM, leveling	1988–1992	5.5	ellipsoidal
Marshall et al. (1997)	GPS	1990–1994	7	ellipsoidal
Thatcher and Massonet (1997)	satellite interferometry	1992–1996	7	ellipsoidal
Battaglia et al. (1999)	gravity, leveling	1982–1998	10–14	spherical
Tiampo et al. (2000)	two-color EDM, leveling	1988–1992	9.9	spherical
Fialko et al. (2001)	two-color EDM, InSAR	1996–1998	7–9	ellipsoidal
this study	two-color EDM, GPS, leveling	1985–1999	4.9–7.6	ellipsoidal

the existence of other inflation sources. We have been able to occupy with GPS only a fraction of 350 leveling bench marks existing in Long Valley, and thus may have missed second-order effects in the deformation field due to less prominent sources (e.g. Marshall et al., 1997), particularly in the south moat.

The association of the active source of inflation found inverting geodetic data with a magma chamber, or anomalies in the crustal structure, is difficult. Inversion of seismic data from Sanders et al. (1994) showed several seismic velocity anomalies beneath the resurgent dome at depths between 6 and 8 km. While the attenuation of P waves at the dome boundary may indicate the presence of supercritical fluids associated with the caldera hydrothermal system, Sanders et al. (1994) related the S wave attenuation to a shallow magmatic system.

While the ellipsoidal model defined in this paper provides a more realistic representation of the Long Valley caldera inflation source than a point source model, there is at least one more factor that should be taken into account when discussing the interpretation of our results. The crust is not a homogeneous half-space. A layered Earth model, with one or more elastic layers may be more realistic, although lateral variations also exist. Does the effect of heterogeneity yield differences in displacement as significant as the differences between spherical and ellipsoidal sources? Numerical experiments by Battaglia and Segall (2004) show no major differences between modeling the intrusion using a point source in a homogeneous or layered medium for an elastic model appropriate to Long Valley caldera. Deformation measurements bound only volume changes within the crust, not the cause of those volume changes. We can better define the deformation source in Long Valley by coupling repeated micro-gravity and deformation measurements (e.g. Battaglia et al., 1999). Before gravity changes can be interpreted, however, they must be corrected for the effects of uplift (the free-air correction) and changes to the depth of the water table (Jachens and Roberts, 1985). In the second paper about the mechanics of unrest at Long Valley caldera (Battaglia et al., 2003 – this issue), we use the uplift

data obtained from differencing GPS and leveling to reduce the gravity data collected in the summer of 1998 and 1999. These reduced gravity data together with the deformation data described here are employed to estimate the density of the intrusion beneath the resurgent dome.

Acknowledgements

References

Bailey, R.A., 1989. Geologic map of Long Valley Caldera, Mono-Inyo Craters volcanic chain, and vicinity, eastern California, Map I-1933. US Geol. Survey, Reston.

Bailey, R.A., Hill, D.P., 1990. Magmatic unrest at Long Valley Caldera, California, 1980–1990. Geosci. Can. 17, 175–179.

Balazs, E.I., Young, G.M., 1982. Corrections applied by the National Geodetic Survey to precise leveling observations. NOAA Technical Memorandum, NOS-NGS 34, 12 pp.

Bar-Sever, Y.E., Kroger, P.M., Borjesson, J.A., 1998. Estimating horizontal gradients of tropospheric path delay with a single GPS receiver. J. Geophys. Res. 103, 5019–5035.

Battaglia, M., Roberts, C., Segall, P., 1999. Magma intrusion beneath Long Valley caldera confirmed by temporal changes in gravity. Science 285, 2119–2122.

Battaglia, M., Segall, P., 2004. The interpretation of gravity changes and crustal deformation in active volcanic areas. Pure Appl. Geophys. 161 (in press).

Battaglia, M., Segall, P., Roberts, C., 2003. The mechanics of unrest at Long Valley caldera, California. 2. Constraining the nature of the source using geodetic and micro-gravity data. J. Volcanol. Geotherm. Res. 127, 219–245.

Berrino, G., Rytmer, H., Brown, C., Corrado, G., 1992. Gravity-height correlations for unrest at calderas. J. Volcanol. Geotherm. Res. 53, 11–26.

Denlinger, R.P., Riley, F.S., 1984. Deformation of Long Val-

ley Caldera, Mono County, California, from 1975 to 1982. J. Geophys. Res. 89, 8303–8314.

Dieterich, J.H., Decker, R.W., 1975. Finite element modeling of surface deformation associated with volcanism. J. Geophys. Res. 80, 4094–4102.

Dixon, T., Mao, A., Bursik, M., Heflin, M., Langbein, J., Stein, R., Webb, F., 1997. Continuous monitoring of surface deformation at Long Valley Caldera, California, with GPS. J. Geophys. Res. 102, 12017–12034.

Efron, B.0., Tibshirani, R., 1986. Bootstrap methods for standard errors, confidence intervals, and other measures of statistical accuracy. Stat. Sci. 1, 54–77.

Estrem, J.E., Lisowski, M., Savage, J.C., 1985. Deformation in the Long Valley Caldera, California, 1983–1984. J. Geophys. Res. 90, 12683–12690.

Fialko, Y., Simons, M., Khazan, Y., 2001. Finite source modelling of magmatic unrest in Socorro, New Mexico, and Long valley, California. Geophys. J. Int. 146, 191–200.

Heiskanen, W., Moritz, H., 1967. Physical Geodesy. W.H. Freeman, San Francisco, CA.

Hill, D.P., Ellsworth, W.L., Johnston, M.J., Langbein, J.O., Oppenheimer, D.H., Pitt, A.M., Reasenberg, P.A., Sorey, M.L., McNutt, S.R., 1990. The 1989 earthquake swarm beneath Mammoth Mountain, California; an initial look at the 4 May through 30 September activity. Bull. Seism. Soc. Am. 80, 325–339.

Jachens, R., Roberts, C., 1985. Temporal and areal gravity investigations at Long Valley Caldera, California. J. Geophys. Res. 90, 11210–11218.

Kahle, J., Bryant, W.A., Hart, E., 1986. Fault rupture associated with the July 21, 1986 Chalfant Valley earthquake, Mono and Inyo counties, California. Calif. Geol. 39, 243–245.

Knesel, K., Davidson, J.P., 1997. The origin and evolution of large-volume silicic magma systems; Long Valley Caldera. Int. Geol. Rev. 39, 1033–1052.

Kotsakis, C., Sideris, M.G., 1999. On the adjustment of combined GPS/levelling/geoid networks. J. Geod. 73, 412–421.

Langbein, J., 1989. Deformation of the Long Valley caldera, eastern California, from mid-1983 to mid-1988: measurements using two-color geodimeter. J. Geophys. Res. 94, 3833–3849.

Langbein, J., Hill, D.P., Parker, T.N., Wilkinson, S.K., 1993. An episode of reinflation of the Long Valley Caldera, eastern California, 1989–1991. J. Geophys. Res. 98, 15851–15870.

Langbein, J., Dzurisin, D., Marshall, G., Stein, R., Rundle, J., 1995. Shallow and peripheral volcanic sources of inflation revealed by modeling two-color geodimeter and leveling data from Long Valley Caldera, California, 1988–1992. J. Geophys. Res. 100, 12487–12495.

Langbein, J., Johnson, H., 1997. Correlated errors in geodetic time series; implications for time-dependent deformation. J. Geophys. Res. 102, 591–604.

Langley, R.B., 1992. Basic geodesy for GPS. GPS World 92, 44–49.

Lichten, S.M., Border, J.S., 1987. Strategies for high-precision global positioning system orbit determination. J. Geophys. Res. 92, 12751–12762.

Marshall, G., Langbein, J., Stein, R.S., Lisowski, M., Svarc, J., 1997. Inflation of Long Valley Caldera, California, basin and range strain, and possible Mono craters dike inflation from 1990–94 GPS surveys. Geophys. Res. Lett. 24, 1003–1006.

McTigue, D.F., 1987. Elastic stress and deformation near a finite spherical magma body; resolution of the point source paradox. J. Geophys. Res. 92, 12931–12940.

Metz, J.M., Mahood, G., 1985. Precursors to the Bishop Tuff eruption; Glass Mountain, Long Valley, California. J. Geophys. Res. 90, 11121–11126.

Milbert, D.G., 1991. Computing GPS-derived orthometric heights with the GEOID90 geoid height model. Technical Papers of the 1991 ACSM-ASPRS Fall Convention. American Congress on Surveying and Mapping, Washington, DC, pp. A46–A55.

Milbert, D.G., 1995. Improvement of a high resolution geoid height model in the United States by GPS height on NAVD 88 bench marks. New geoids in the world, Bulletin d'Information, Bureau Gravimetrique International, 0373-9023, 77, pp. 13–36.

Milbert, D.G., Smith, D.A., 1996. Converting GPS Height into NAVD 88 Elevation with the GEOID96 Geoid Height Model. GIS/LIS '96 Annual Conference and Exposition. American Congress on Surveying and Mapping, Washington, DC, pp. 681–692.

Nishi, K., Ono, H., Mori, H., 1999. Global positioning system measurements of ground deformation caused by magma intrusion and lava discharge: the 1990–1995 eruption at Unzendake volcano, Kyushu, Japan. J. Volcanol. Geotherm. Res. 89, 23–34.

Rapp, R.H., 1980. Precise definition of the geoid and its realization for vertical datum applications. NAD Symposium, Ottawa, pp. 73–86.

Rothacher, M., Schaer, S., Beutler, G., Schülter, W., Hase, H.O., 1996. Phase center variations of GPS antennas derived from GPS observations of specially designed calibration campaigns. EOS 77, G11A-6.

Rymer, H., 1994. Microgravity change as a precursor to volcanic activity. J. Volcanol. Geotherm. Res. 61, 311–328.

Sanders, C.O., Ponko, S.C., Christopher, O., 1994. Inversion for P and S wave attenuation structure, Long Valley Caldera, California. J. Geophys. Res. 99, 2619–2635.

Savage, J.C., 1988. Principal component analysis of geodetically measured deformation in Long Valley Caldera, eastern California, 1983–1987. J. Geophys. Res. 93, 13297–13305.

Savage, J.C., Cockerham, R., 1984. Earthquake swarm in Long Valley Caldera, California, January 1983: evidence for dike inflation. J. Geophys. Res. 89, 8315–8324.

Savage, J.C., Cockerham, R., Estrem, J.E., Moore, L.R., 1987. Deformation near the Long Valley Caldera, eastern California, 1982–1986. J. Geophys. Res. 92, 2721–2746.

Segall, P., Matthews, M.V., 1988. Displacement calculations from geodetic data and the testing of geophysical deformation models. J. Geophys. Res. 93, 14594–14966.

Sieh, K., Bursik, M.I., 1986. Most recent eruption of the Mono Craters, eastern Central California. J. Geophys. Res. 91, 12539–12571.

Smith, D., Milbert, D.G., 1999. The GEOID96 high-resolution geoid height model for the United States. J. Geod. 73, 219–236.

Smith, D., Roman, D., 1999. GEOID99 (CD-ROM). National Geodetic Survey, Silver Spring, MD.

Snay, A., Soler, T., 2000. Modern Terrestrial reference Systems, part 3: WGS84 and ITRS. Prof. Surv. 3, 1–3.

Sorey, M.L., Kennedy, B.M., Evans, W.C., Farrar, C.D., Suemnicht, G.A., 1993. Helium isotope and gas discharge variations associated with crustal unrest in Long Valley Caldera, California, 1989–1992. J. Geophys. Res. 98, 15871–15889.

Thatcher, W., Massonet, D., 1997. Crustal deformation of Long Valley Caldera, eastern California, 1992–1996, inferred from satellite radar interferometry. Geophys. Res. Lett. 24, 2519–2522.

Tiampo, K.F., Rundle, J.B., Fernandez, J., Langbein, J., 2000. Spherical and ellipsoidal volcanic sources at Long Valley caldera, California, using a genetic algorithm inversion technique. J. Volcanol. Geotherm. Res. 102, 189–206.

van den Bogaard, P., Schirnick, C., 1995. $^{40}Ar/^{39}Ar$ laser probe ages of Bishop Tuff quartz phenocrysts substantiate long-lived silicic magma chamber at Long Valley, United States. Geology 23, 759–762.

Yang, X., Davis, P.M., Dieterich, J.H., 1988. Deformation from inflation of a dipping finite prolate spheroid in an elastic half-space as a model for volcanic stressing. J. Geophys. Res. 93, 4249–4257.

Zilkoski, D.B., D'Onofrio, J.D., Frakes, S.J., 1997. Guidelines for establishing gps-derived ellipsoid heights (standards: 2 cm and 5 cm). Version 4.3. NOAA Technical Memorandum NOS NGS-58, Silver Spring, MD.

Zilkoski, D.B., Richards, J.H., Young, G.M., 1992. Results of the general adjustment of the North American Vertical datum of 1988. Surv. Land Inf. Syst. 52, 133–149.

Zumberge, J.F., Heflin, M.B., Jefferson, D.C., Watkins, M.M., Webb, F.H., 1997. Precise point positioning for the efficient and robust analysis of GPS data from large networks. J. Geophys. Res. 102, 5005–5017.